Heliyon 8 (2022) e12493

Contents lists available at ScienceDirect

Heliyon

journal homepage: www.cell.com/heliyon

Research article

Analysis of optimal detection range performance of LiDAR systems applying coaxial optics

Duck-Lae Kim *, Hyun-Woo Park, Yoon-Mo Yeon

LIG Nex1, EO/IR Systems R&D, 207 Mabuk-ro, Yongin-si, 16911, South Korea

ARTICLE INFO

Keywords:
Sensors
Lasers
LiDAR
MEMS mirror

ABSTRACT

In this study, the optimal detection range performance of a LiDAR system employing coaxial optics is analyzed. On analyzing laser beam diameter, beam divergence angle, light-receiving area, and receiving light intensity, the optimal detection range was exhibited when the collimator focal length was 6.5 mm, the laser-beam divergence angle was 1.23 mrad, and the hole of the receiving mirror was 1.4 mm. Furthermore, the maximum deviation of the optical scan angles with respect to the mechanical angles of the polygon mirror and the MEMS mirror were analyzed as -0.99° and +4.54° in the x-axis and y-axis directions, respectively.

1. Introduction

Many companies such as Volvo, Audi, Volkswagen, and Hyundai Motors use expensive laser imaging, detection, and ranging (LiDAR) systems in addition to cameras for autonomous driving because there is a limit to recognizing a surrounding environment using only camera image information. The reliability of autonomous driving can be improved by acquiring 3D image information using LiDAR sensors [1, 2]. To design a vehicle-mounted LiDAR system, the operation mechanisms of its core parts need to be selected considering the embedding. The laser light source should be selected considering the scanning performance, the machine design; the driving environment of the vehicle, and the optical path; the characteristics of the laser light detection. The designs of the optical driving part should be based on detection of wide angles.

Solid-state LiDARs using micro-electro-mechanical-system (MEMS) mirrors or vertical-cavity surface-emitting lasers have more advantages than rotating LiDARs in terms of embedding and the operation mechanisms of key components [3, 4]. To use a MEMS mirror in a LiDAR, the performance of the single crystal silicon torsional bars in the chip unit, fatigue and durability of the spring, and vibration and shock absorption performance of the MEMS-mirror packaging unit must all be satisfactory [5, 6, 7]. Most commercially available MEMS mirrors have diameters from 1 mm to 3 mm and resonant frequencies varying from several kilohertz to 30 kHz. In MEMS mirrors, the resonant frequency decreases as the diameter increases. In other words, simultaneously increasing the resonant frequency and diameter of a MEMS mirror is difficult [8, 9, 10].

Concerning scanning performance, a 1550-nm laser beam is not only more effective than a 905-nm laser beam for atmospheric transmission and solar noise but also safer for the eyes [11, 12, 13]. Among various laser sources, a fiber laser can improve the detection range of a LiDAR because it can obtain a peak power of several kilowatts higher than that of a laser diode. A fiber laser can be used to design a collimator having a small laser beam diameter and beam divergence angle because a fiber laser exhibits a good beam-quality-factor (M^2) of 1.5 or less. These advantages can contribute to improvements in the spatial resolution of a LiDAR. In optical fiber lasers, output energy decreases with pulse repetition rate. However, the LiDAR resolution can be controlled because a repetition rate of several megahertz can be obtained. To ensure the reliability of a LiDAR system when operated on rough terrains for a long time, structural analysis and thermal analysis results should be applied considering the temperature, humidity, vibration, and impact of the target outdoor operating environment in the machine design.

In an optical-driver design for wide-angle detection and scanning, the LiDAR system generally comprises polygon mirrors or prisms to scan wide angles of more than 100° in the horizontal direction. Additionally, a MEMS mirror is used to scan more than 20° in the vertical direction. In a LiDAR system in which the transmitter and receiver units are separated, the position of the laser spot received by the photodetector moves according to the scan angle of the LiDAR system. A photodetector having a wide detection surface or an array-type photodetector must be used to detect a mobile laser spot. A wide photodetector with an effective diameter of 3 mm or more has a rising time of several tens of nanoseconds

* Corresponding author.
E-mail addresses: kimducklae@lignex1.com, ducklaekim@gmail.com (D.-L. Kim).

https://doi.org/10.1016/j.heliyon.2022.e12493
Received 6 October 2022; Received in revised form 11 November 2022; Accepted 13 December 2022
2405-8440/© 2022 The Author(s). Published by Elsevier Ltd. This is an open access article under the CC BY-NC-ND license (http://creativecommons.org/licenses/by-nc-nd/4.0/).

or more. Therefore, the detection range of the LiDAR system decreases when the response time for a laser pulse with a width of 1 ns increases. Using an array detector is unfavorable because the fill factor is lowered due to the array pitch, resulting in optical loss. This degradation in performance of the LiDAR system can be solved by using coaxial optic fibers having the same optical axis as the transmitter and receiver. When coaxial optics is employed, a single element photodetector with a small effective diameter can be used because the spot position of the received light does not move even when the scan angle of the LiDAR system is changed. Furthermore, the single-element photodetector can improve the detection range performance because it has a short response time of 1 ns or less. Coaxial optics has the advantage of being able to transmit and receive signals in a wide area. However, it is necessary to design an optimal LiDAR system because the detection range performance of a LiDAR system varies depending on the diameter and divergence angle of the laser beam output from the laser collimator and the light receiving area of the receiver.

This study analyzed the laser beam diameter, beam divergence angle, and light receiving area of coaxial optic fibers according to collimator design by combining the factors that are considered while designing a vehicle-mounted LiDAR system. Moreover, the detection range performance of the LiDAR system was optimized by analyzing the received laser-light intensity reflected from the target. In addition, the deviation of the optical scan angle with respect to the mechanical angle of a polygon mirror and MEMS mirror was analyzed.

2. Composition of the LiDAR system

Figure 1 shows the configuration diagram of the LiDAR system. The laser beam output from the fiber laser passes through the hole of the receiving mirror. Next, it is reflected by the MEMS mirror and polygon mirror. The target is irradiated by the laser beam at a scan frequency of 15 Hz, horizontal angular resolution of 0.1°, and vertical angular resolution of 0.4°. The laser beam reflected from the target is reflected onto the outer parts of the pentagonal polygon mirror, except on its hole, one dimensional (1D) MEMS mirror, and receiving mirror and is focused

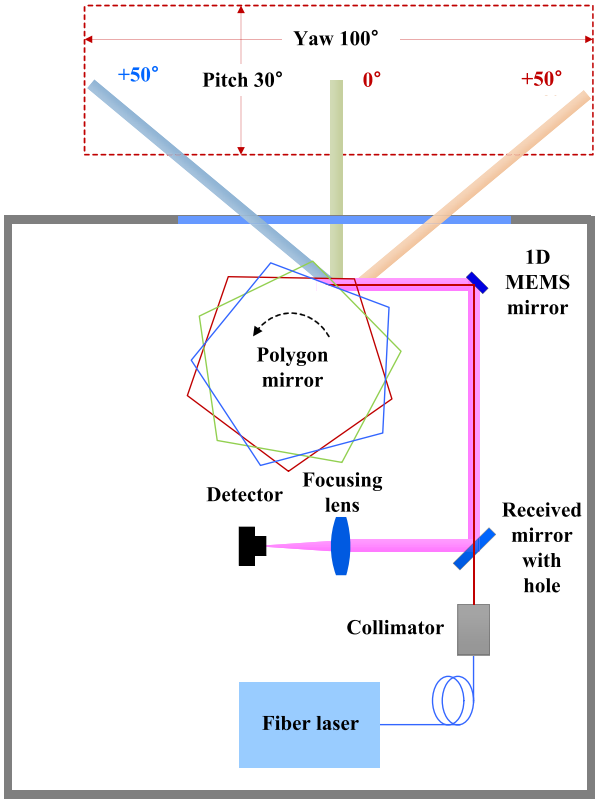

Figure 1. Configuration of the LiDAR system applying coaxial optics.

Table 1. Collimator specifications.

No.	EFL	1 side radius of curvature	2 side radius of curvature	Thickness	Material
Case 1	4.5 mm	Infinity	-2.25 mm	2.5 mm	NBK7
Case 2	6.5 mm	Infinity	-3.25 mm	2.5 mm	NBK7
Case 3	8.5 mm	Infinity	-4.26 mm	2.5 mm	NBK7

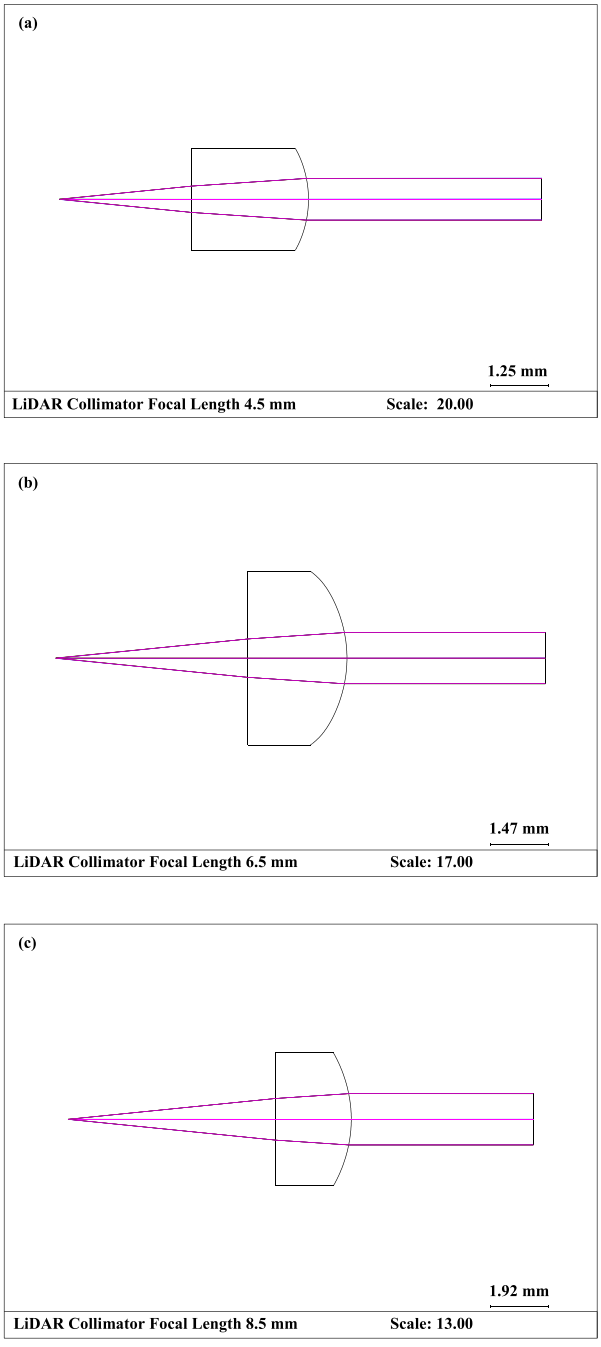

Figure 2. Collimator layouts under three different focal lengths; (a) EFL 4.5 mm, (b) EFL 6.5 mm, (c) EFL 8.5 mm.

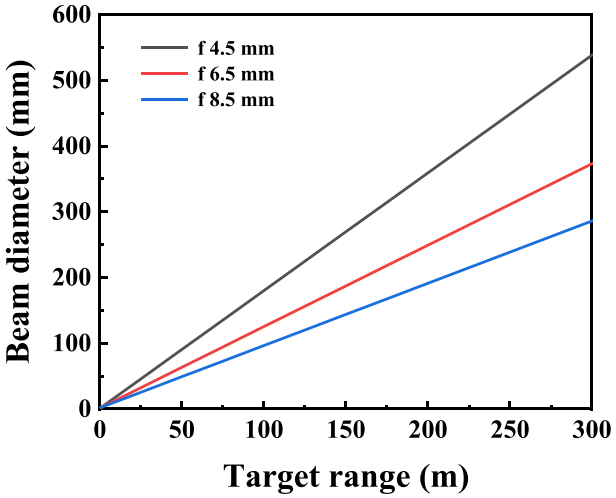

Figure 3. Beam diameter for target distance by focal distance of collimator.

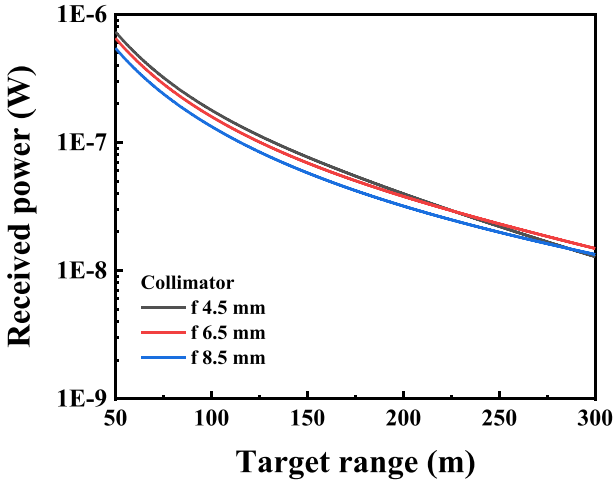

Figure 4. Received power against the target range by focal length of collimator.

onto the photodetector through an optical system. The amount of light received from the target and directed to the focusing optical system is the difference of the amount of light through the hole-area of the receiving mirror from the amount of light reflected on the effective area of the MEMS mirror.

The specifications of each component for detection range analysis are as follows. Considering atmospheric transmittance, the wavelength of the fiber laser was 1550 nm. Considering the detection range, the laser beam quality factor was 1.2, the output energy was 1.5 μJ; considering the scan frequency of the LiDAR system, the pulse repetition rate was 1.62 MHz, and the pulse width was 1.0 ns. The amplified signal from an optical fiber amplifier is transferred to a transmission optical fiber with a core diameter of 8 μm and a numerical aperture of 0.1. The MEMS mirror performs 1-D scans in the vertical direction. The optical vertical scan angle was 30°. Considering the scan frequency, the effective diameter and resonance frequency of the MEMS mirror were 3 mm and 10.8 kHz (= 72°/50° x 15 Hz x 1000 points/2), respectively, and its reflectance was more than 95% at 1550 nm, the laser wavelength. The pentagonal polygon mirror rotates three times per second in the horizontal direction; its optical horizontal scan angle was 100°, and the duty rate of the effective optical scan angle with respect to the mechanical rotation angle was 69.4%. The single-chip photodetector used was an InGaAs avalanche photodiode, which has high responsivity in the wavelength band of 1550 nm. It had an active diameter of 75 μm, a bandwidth of more than 2 GHz, and a minimum detectable signal of less than 20 nW [14], based on the noise of the photodetector and signal processing board. The detection range of a LiDAR system can be increased or decreased depending on atmospheric conditions and component performance. The extinction coefficient was set to 1.0 x 10^{-14} $m^{-2/3}$ at 0.196 km^{-1} under clear weather conditions, taking into account the ground operating conditions for the refractive index structure [15]. Here, the refractive index structure is a parameter representing atmospheric turbulence, which causes the laser beam to wander and the beam diameter at the target and divergence angle of the laser beam to increase. Hence, it affects the detection range performance. The target reflectance was 80%, and the target size analyzed was in a range in which the length of one side of a square target was between 0.10 m and 1.58 m.

Table 2. Parameters of the detection-range calculation.

Description	Symbol	Value
Laser energy per pulse	E_{Pulse}	1.5 μJ
Laser pulse width	Δt	1 ns
Laser efficiency	τ_{Tx}	0.95
Laser wavelength	λ	1550 nm
Extinction coefficient	α	0.057 km^{-1}
Target hemispherical reflectivity	ρ	0.8
Laser jitter	δ_j	50 mrad
Refractive index structure constant	C_n^2	4×10^{-14} $m^{-2/3}$
Receiver efficiency	τ_{Rx}	0.8

3. Analysis

3.1. Optimization of detection range performance of the LiDAR system according to collimator design

We used Code V, a commercial optical design software, to create the layout of the collimator. While designing the collimator, the height of the object plane was set to 8 μm, the same as the core diameter of the transmission optical fiber. The angle of the beam emitted from the cross section of the optical fiber was set to 0.1 NA, which was equal to the numerical aperture of the optical fiber. An aspherical surface was introduced on both surfaces of each lens.

Three cases of collimator effective focal lengths (EFLs) were analyzed: 4.5 mm, 6.5 mm, and 8.5 mm. Considering the diameter of the laser beam 10 mm away from the collimator, three hole-diameters of the receiving mirror was analyzed: 1.0 mm, 1.4 mm, and 1.8 mm.

As the focal length of the collimator increased, the diameter of the laser beam emitted from the collimator also increased. Therefore, the

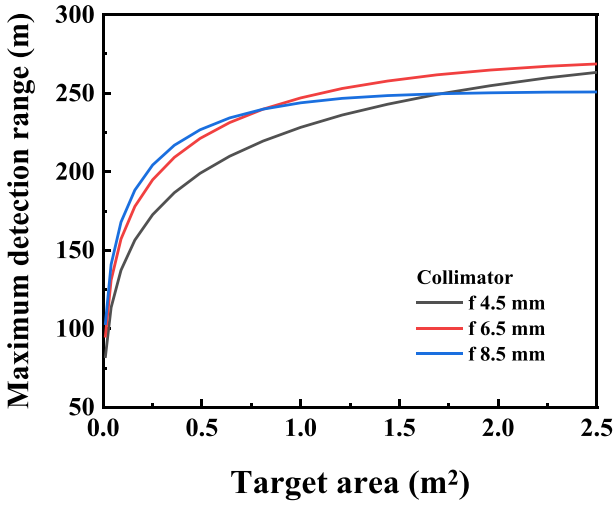

Figure 5. Maximum detection range by target area for each collimator.

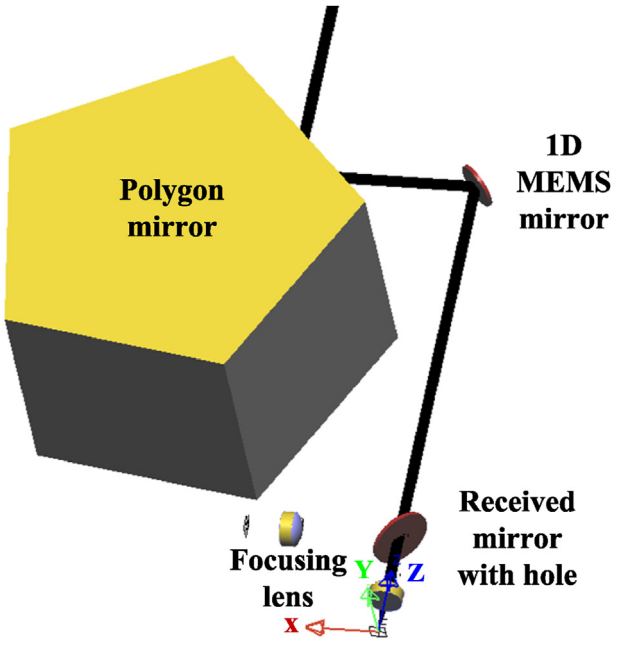

Figure 6. Light path diagram of the laser beam.

hole of the receiving mirror became larger, and lesser area received the light from the target. In contrast, as the focal length of the collimator increased, the divergence angle of the laser beam decreased, the power per unit area irradiated to the target increased, and the probability of light loss due to target-splitting effects decreased.

The specifications of the collimators are listed in Table 1. The diameter and divergence angle of the laser output beam from the collimator are described in detail in Figure 2. A collimator with an EFL of 4.5 mm and the total divergence angle of 1.78 mrad is shown in Figure 2(a). A collimator with an EFL of 6.5 mm and the total divergence angle of 1.23 mrad is shown in Figure 2(b). A collimator with an EFL of 8.5 mm and the total divergence angle of 0.94 mrad is shown in Figure 2(c).

A plot of the beam diameter, for each focal length, with respect to the target range is shown in Figure 3. For a collimator with an EFL of 4.5 mm, the laser-beam diameter was 0.92 mm at a distance of 10 mm from the collimator. In other words, the hole of the receiving mirror needed to be 1.0 mm. Excluding atmospheric effects, the beam diameter was 300 mm at a target range of 167 m. For a target size of 0.3 × 0.3 m, laser beam splitting occurred at a target range of 167 m or more. With a 6.5-mm EFL collimator, the diameter of the laser beam at the receiving mirror was 1.31 mm; hence, the required diameter of the hole of the receiving mirror was 1.31 mm. With an 8.5-mm EFL collimator, the required diameter of the hole of the receiving mirror was 1.8 mm. For collimators with EFLs of 6.5 mm and 8.5 mm, laser beam splitting occurred over target ranges of 241 m and 315 m, respectively, for a target size of 0.3 × 0.3 m.

The detection range is calculated as below [16].

$$P_{Rx} = \left(\frac{E_{Pulse}}{\Delta t}\tau_{Tx}\right)\exp(-\alpha R)\rho \int_{-\frac{H}{2}}^{\frac{H}{2}} \times \int_{-\frac{W}{2}}^{\frac{W}{2}} \frac{e^{-\left(\frac{x^2}{2R^2\delta}+\frac{y^2}{2R^2\delta}\right)}}{2\pi R\sqrt{\delta}} dxdy \exp(-\alpha R)\left(\frac{\pi(D_{Rx}/2)^2}{\pi R^2}\right)\tau_{Rx} \quad (1)$$

where E_{Pulse} represents laser output energy, Δt represents laser pulse width, τ_{Tx} represents the transmissivity of the transmitting part of the optical system, α represents the atmospheric air extinction coefficient between the LiDAR and the target, R represents the distance between the LiDAR and the target, ρ represents the target reflectivity, and H and W represent the height and width of the footprint, respectively. D_{Rx} represents the diameter of the entrance pupil of the LiDAR, and τ_{Rx} represents the transmissivity of the receiving part of optical system. The jitter of the LiDAR is expressed as $\delta = \delta_b^2 + \delta_j^2 + \delta_i^2$, where δ_b represents the laser beam divergence, δ_j represents the jitter of the transmitter, and δ_i =

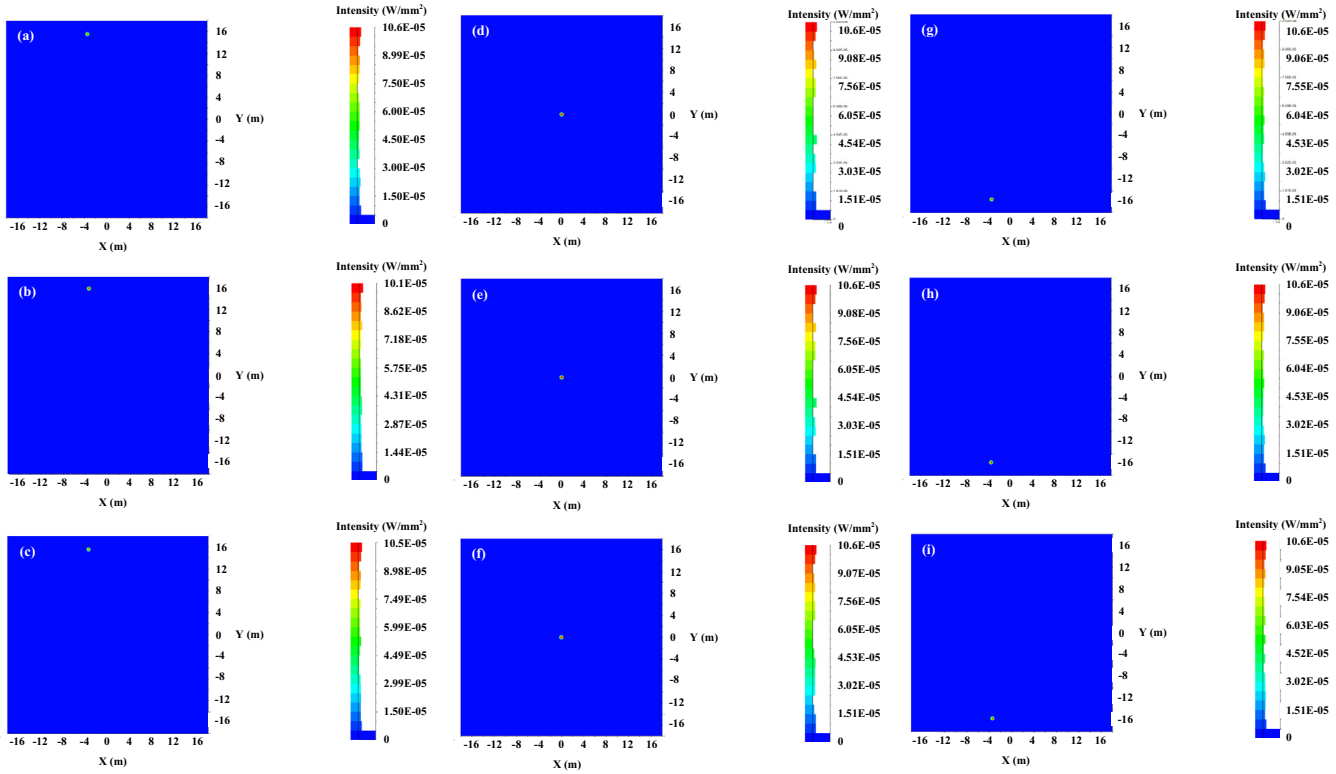

Figure 7. Laser spots at the target for the scan angles of the LiDAR system.

$3.98\sqrt{(1/\lambda)^{2/5}(C_n^2)^{6/5}R^{16/5}}/R$. Here, λ is the laser wavelength, and C_n^2 is the refractive index structure function. The parameters of the detection-range calculation are listed in Table 2.

A plot of the LiDAR received power with respect to the target range for each EFL of the collimator is shown in Figure 4. The received power was calculated using Eq. (1) with a target size of 1.5 m × 1.5 m. At a target range of 50 m, when the EFLs were 4.5 mm, 6.5 mm and 8.5 mm, the received light intensities of the LiDAR system were 730.0 nW, 650.6 nW and 544.5 nW, respectively. Hence, the collimator with an EFL of 4.5 mm facilitated the highest received light intensity. At a target range of 226.5 m, the LiDAR system with EFLs of 4.5 mm and 6.5 mm exhibited a received light intensity of 28.9 nW; when the EFL was 8.5 mm, the received light intensity was 24.5 nW. At a target range of 300 m, the received light intensities of LiDAR system were 12.8 nW, 14.8 nW, and 13.3 nW when the EFLs were 4.5 mm, 6.5 mm, and 8.5 mm, respectively. Therefore, the collimator with an EFL of 6.5 mm facilitated the highest received light intensity. In the near target range of 50 m, the beam loss of the receiving mirror, rather than the beam loss at the target, affected the received light intensity due to the divergence angle. Analysis results show that as the target range increased to more than 200 m, the divergence angle of the laser beam affected the received light intensity. To determine the optimal EFL, the detection range of LiDAR system according to the target size was analyzed.

A plot of the maximum detection range of the LiDAR system with respect to the target area and collimator is shown in Figure 5. The target shape was assumed to be square. When the length of one side of the target was increased from 0.10 m to 1.58 m, the maximum target area was 2.5 m^2. When the target area was 0.81 m^2 or less, the received signal was the highest when the collimator with a focal length of 8.5 mm was used. For a target area of 0.81 m^2 or more, the received signal was the highest when the collimator with a focal length of 6.5 mm was used. The detection range calculation results according to the target area can be analyzed as follows. The beam reflected from the target was reflected by the polygon mirror, the MEMS mirror, and the receiving mirror; next, it was received by the detector. If the target is small, reducing the beam divergence angle is effective even if light loss due to the hole of the receiving mirror is taken into account. If the target is large, reducing the light loss due to the hole of the receiving mirror is effective even if the beam divergence angle is large. However, when the collimator with an effective focal length of 4.5 mm was used, the light loss was considerable because the beam size at the target was larger than the target size. When various target sizes were analyzed, it was found that the most suitable collimator for the LiDAR system with coaxial optics had a focal length of 6.5 mm. The detection range was analyzed to be 267.2 m when the area of the target was 2.25 m^2 with the collimator with an effective focal length of 6.5 mm.

3.2. Deviations of optical scan angle with respect to the mechanical angles of polygon and MEMS mirrors

The pitch axis and yaw axis coordinates of the laser spot on the target according to changes in the mechanical angle of the MEMS and polygon mirrors were analyzed using Light Tools, a commercial software application. In Figure 6, the path of a laser beam as it irradiates a target after reflection from the MEMS and polygon mirrors is illustrated.

The laser spots at the target for the pitch and yaw angles of the LiDAR system is shown in Figure 7. For calculating the spot position, coordinate signs were defined as positive for clockwise and upward directions and negative for counterclockwise and downward directions, based on the 0° of both yaw axis and pitch axis. A laser spot at −50° on the yaw axis and 15° on the pitch axis is shown in Figure 7(a); a laser spot at 0° on the yaw axis and 15° on the pitch axis is shown in Figure 7(b); a laser spot at 50° on the yaw axis and 15° on the pitch axis is shown in Figure 7(c); a laser spot at −50° on the yaw axis and 0° on the pitch axis is shown in Figure 7(d); a laser spot at 0° on the yaw axis and 0° on the pitch axis is shown in Figure 7(e); a laser spot at 50° on the yaw axis and 0° on the pitch axis is shown in Figure 7(f); a laser spot at −50° on the yaw axis and at −15°on the pitch axis is shown in Figure 7(g); a laser spot at 0° on the yaw axis and at −15°on the pitch axis is shown in Figure 7(h); a laser spot at 50° on the yaw axis and at −15°on the pitch axis is shown in Figure 7(i). As shown in Figure 7, when the pitch axis was 0°, the laser spot did not deviate even when the angle on the yaw axis was changed. However, the spot deviated when the pitch axis was either 15° or −15°. This phenomenon was caused by the deviation of the reflection position of the laser as the scan angle of the polygon mirror varied and the roll axis error, generated due to the combined effects of the tilt of the MEMS mirror in the pitch axis and rotation of the laser beam reflected from the polygon mirror in the yaw axis. This is quantitatively explained in detail in Figure 8.

The deviation of the pitch angle of the MEMS mirror is shown Figure 8 when the yaw angle of the polygon mirror was −50°. As shown in Figure 8(a), as the pitch angle of the MEMS mirror changed from −15° to 0°, the deviation in the x-axis direction changed from −0.98° to 0°. As the angle of the MEMS mirror changed from 0° to +15°, the deviation again changed from 0° to −0.98°. As shown in Figure 8(b), as the angle of the MEMS mirror changed from +15° to −15°, the deviation in the y-axis direction changed from −4.45° to +4.45°. In all cases, deviation tended to occur in the negative direction according to the change in the pitch angle of the MEMS mirror even at angles 0° and +50° on the yaw axis. This can also be seen in Figure 7. This angular deviation caused a position error, which should be compensated as much as possible by controlling the polygon and MEMS mirrors. The deviation values according to the

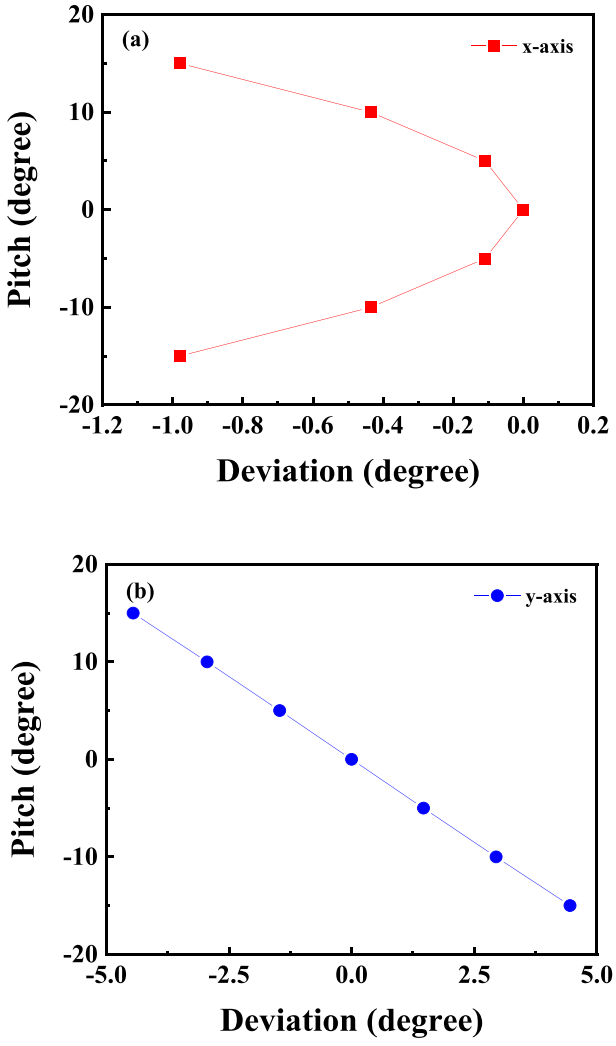

Figure 8. Deviations of x-axis (a) and y-axis (b) according to the pitch angle at the yaw angle of -50°.

Table 3. Deviations of x-axis and y-axis for yaw and pitch angles.

Yaw	-50°		0°		+50°	
Pitch	x-axis	y-axis	x-axis	y-axis	x-axis	y-axis
15°	-0.98°	-4.45°	-0.98°	-4.45°	-0.98°	-4.45°
10°	-0.44°	-2.95°	-0.44°	-2.95°	-0.44°	-2.95°
5°	-0.11°	-1.47°	-0.11°	-1.47°	-0.11°	-1.47°
0°	0.00°	0.00°	0.00°	0.00°	0.00°	0.00°
-5°	-0.11°	1.47°	-0.11°	1.47°	-0.11°	1.47°
-10°	-0.44°	2.95°	-0.44°	2.95°	-0.44°	2.95°
-15°	-0.98°	4.45°	-0.99°	4.54°	-0.98°	4.45°

changes in the yaw angle of the polygon mirror and the pitch angle of the MEMS mirror are listed in Table 3.

4. Conclusions

In this study, the optimal detection range performance of a LiDAR system with coaxial optics, on the basis of the laser beam diameter, beam divergence angle, light receiving area, and received laser-light intensity was analyzed. The LiDAR system showed an optimal performance when the focal length of the collimator was 6.5 mm, the beam divergence angle was 1.23 mrad, and the hole of the receiving mirror was 1.4 mm. The detection range was analyzed to be 267.2 m when the area of the target was 2.25 m^2. The deviation of the optical scan angle with respect to the changes in the mechanical angle of the polygon and MEMS mirrors was analyzed. As the pitch axis changed from $+15^\circ$ to -15°, the x-axis deviation was -0.99° at the maximum, and the y-axis deviation ranged from -4.45° to $+4.54^\circ$. Further research on angular deviation compensation is necessary to improve the reliability of a LiDAR system in the future.

Declarations

Author contribution statement

Duck-Lae Kim, Hyun-Woo Park; Yoon-Mo Yeon: Conceived and designed the experiments; Performed the experiments; Analyzed and interpreted the data; Contributed reagents, materials, analysis tools or data; Wrote the paper.

Funding statement

This research did not receive any specific grant from funding agencies in the public, commercial, or not-for-profit sectors.

Data availability statement

Data will be made available on request.

Declaration of interest's statement

The authors declare no competing interests.

Additional information

No additional information is available for this paper.

References

[1] H.W. Yoo, N. Druml, D. Brunner, C. Schwarzl, T. Thurner, M. Hennecke, G. Schitter, MEMS-based lidar for autonomous driving, Elektrotech. Inf. 135 (6) (2018) 408–415.
[2] H. Wang, B. Wang, B. Liu, X. Meng, G. Yang, Pedestrian recognition and tracking using 3D LiDAR for autonomous vehicle, Robot. Autonom. Syst. 88 (2017) 71–78.
[3] J.Y. Hwang, J.U. Bu, C.H. Ji, Low power electromagnetic scanning micromirror for LiDAR system, IEEE Sensor. J. 21 (6) (2021) 7358–7366.
[4] J. Wang, G. Zhang, Z. You, UKF-based MEMS micromirror angle estimation for LiDAR, J. Micromech. Microeng. 29 (2019), 035005.
[5] S.H. Chung, S.K. Lee, C.H. Ji, J.H. Park, Vacuum packaged electromagnetic 2D scanning micromirror, Sens. Actuators, A 290 (2019) 147–155.
[6] S. Ju, H. Jeong, J.H. Park, J.U. Bu, C.H. Ji, Electromagnetic 2D scanning micromirror for high definition laser projection displays, IEEE Photon. Technol. Lett. 30 (23) (2018) 2072–2075.
[7] H. Jeong, C.H. Ji, S.K. Lee, J.H. Park, High-reflectivity electromagnetic two-axis microscanner using dielectric multi-layer reflective surface, Sens. Actuators, A 276 (2018) 186–195.
[8] D. Wang, C. Watkins, H. Xie, MEMS mirrors for LiDAR: a review, Micromachines 11 (5) (2020) 456.
[9] S.Y. Kang, J.H. Park, C.H. Ji, Design optimization of a 6.4 mm-diameter electromagnetic 2D scanning micromirror, Opt Express 28 (21) (2020) 31272–31286.
[10] A. Han, A.R. Cho, S. Ju, S.H. Ahn, J.U. Bu, C.H. Ji, Electromagnetic biaxial vector scanner using radial magnetic field, Opt Express 24 (14) (2016) 15813–15821.
[11] D.L. Kim, B.H. Jung, H.B. Kong, C.M. Ok, S.T. Lee, Common optical system for the fusion of three-dimensional images and infrared images, Curr. Opt. Photon. 3 (1) (2019) 8–15.
[12] H. Weichel, Laser Beam Propagation in the Atmosphere, SPIE - The International Society for Optical Engineering, 1990.
[13] D.L. Kim, H.B. Kong, S.T. Lee, Effects of solar noise on the detection range performance of a laser spot tracker, Opt. Eng. 60 (3) (2021), 037102.
[14] P.F. McManamon, P.S. Banks, J.D. Beck, D.G. Fried, A.S. Huntington, E.A. Watson, Comparison of flash lidar detector options, Opt. Eng. 56 (3) (2017), 031223.
[15] G.C. Holst, Holst's Practical Guide to Electro-Optical Systems, JCD Publishing, 2003.
[16] M. Friedman, J. Hixson, Q. Nguyen, The Night Vision Laser Designator NVLaserD Users Manual (U. S. ARMY RDECOM, CERDEC, Night Vision and Electronic Sensors Directorate Modeling and Simulation Division, 2006.